THE ASTROPHYSICAL JOURNAL, 382:100–107, 1991 November 20

POLARIZED RADIO EMISSION FROM THE EDGE-ON SPIRAL GALAXIES NGC 891 AND NGC 4565

S. SUKUMAR[1]
Astronomy Department, University of Illinois, 1002 West Green Street, Urbana, IL 61801
AND
R. J. ALLEN[1]
Space Telescope Science Institute, 3700 San Martin Drive, Baltimore, MD 21218
Received 1991 March 26; accepted 1991 May 31

ABSTRACT

The distribution of radio continuum intensity and linear polarization has been observed with the VLA in two nearby edge-on spiral galaxies NGC 891 and NGC 4565 at 6 and 20 cm, respectively. We present here the results at a resolution of 20″. The linearly polarized emission has been measured at high Z-distances of up to ~ 2 kpc, where the degree of polarization increases to over 30%. Although the distribution of polarized emission is nearly symmetric in Z about the major axis for both galaxies, a strong asymmetry about the minor axis is evident in NGC 4565 where the polarized emission at 20 cm appears mostly on the east side of the nucleus. In NGC 891 the distribution of polarized emission at 6 cm is more symmetrically disposed about the minor axis. For both galaxies, the position angle of maximum polarization is generally perpendicular to the plane of the disk. In the 6 cm data of NGC 891, an anomalous region situated at ~ 3 kpc to the northeast of the nucleus shows highly aligned magnetic fields running across the galactic disk.

We present a unified model to account for the main features of the radio polarization in these two edge-on galaxies. The model geometry is determined from recent observations of face-on galaxies where the polarized emission is found to be strongest in the dark inter-arm and outer parts of the disks. We ascribe a substantial Z-thickness to this polarized emission. The asymmetries observed in the distribution of polarized emission when the model is viewed edge-on are a consequence of depolarization over the observing beam by differential Faraday rotation in an intervening plasma with randomly oriented magnetic fields. We show that the exceptionally strong wavelength dependence of this type of Faraday depolarization can result in edge-on galaxies becoming rapidly "Faraday thick" at decimeter wavelengths, thereby obliterating the polarization from regions on the far side of the disk. High-resolution radio polarization observations at several wavelengths can in fact be used together with optical emission-line maps to provide estimates of the line-of-sight average strength and distribution of the magnetic field in these galaxies.

The degree of polarization observed in both galaxies increases strongly with increasing Z-distance from the plane. The low degree of polarization near $Z = 0$ is due to turbulent processes in the interstellar medium of the thin disk which tangle the magnetic field on scales of 100 pc. The intrinsic direction of the magnetic field in both galaxies at high Z is nearly parallel to the plane in the central regions of the disks. In NGC 891 the field lines tilt away from the plane of the galaxy at large distances along the major axis.

Subject headings: galaxies: individual (NGC 891, 4565) — galaxies: interstellar matter — interstellar: magnetic fields — polarization — radio sources: galaxies

1. INTRODUCTION

The volume emissivity of the nonthermal synchrotron radio radiation emanating from the interstellar matter in galaxies depends on the density of relativistic electrons and their energy distribution, as well as on the strength of the magnetic field. The linearly polarized component of this emissivity provides information on the degree of order in the magnetic field, its direction, and on the depolarizing effects of ionized gas present along the line of sight.

Recent studies of the radio continuum polarization in nearby spiral galaxies have significantly improved our understanding of the morphology of ordered magnetic fields in the galactic disks (see the reviews by Sofue, Fujimoto, & Wielebinski 1986; Wielebinski 1990; Beck 1991). From relatively low-resolution data we know that the direction of the field is clearly aligned with the spiral structure of the galaxy (e.g., Sukumar, Klein, & Gräve 1987; Fujimoto 1987; Sofue 1987). However, observations of M83 with resolution sufficient to separate spiral arms from the underlying disk emission provided the surprising result (Sukumar & Allen 1989a) that the degree of polarization was greatest in the dark interarm and outer regions of that galaxy and not at all on the visible spiral as had been surmised. This characteristic of the radio polarization has also been recognized in M51 (Horellou, Beck, & Klein 1990) and M81 (Krause, Beck, & Hummel 1989). Our explanation for this phenomenon (Sukumar & Allen 1989a) is that turbulence associated with the star formation process tangles the magnetic field in the interstellar medium on the scale of 100 pc or so, and it is only in the more quiescent regions where the magnetic field is able to retain a large-scale order.

What is the Z-structure of this polarized emission? The answer to this question would provide the information necessary to determine the intrinsic direction of the magnetic field at

[1] National Center for Supercomputing Applications, University of Illinois.

high Z, a result which is of great interest to theories of the generation of magnetic fields on the galactic scale. Edge-on galaxies are the most obvious candidates for study here, and the observations of NGC 4631 (Hummel et al. 1988) provided striking evidence for the existence of ordered magnetic fields at Z-distances of up to 6.5 kpc. In this paper, we extend the sample to include NGC 891 and NGC 4565. In the order mentioned, these three-edge-on galaxies form a sequence of optical images with decreasing axial ratios, and so provide a range of intrinsic spatial structure of the interstellar gas.

Both NGC 891 and NGC 4565 are classified as late- to intermediate-type spirals having very prominent dust lanes running across their disks. The optical parameters of the galaxies are summarized in Table 1. The distances assumed here are based on a Hubble constant of 100 km s^{-1} Mpc^{-1} and have been chosen to facilitate comparison with other work already in the literature. The high inclination ($>88°$) and high radio surface brightness of NGC 891 make it an ideal candidate for a study of the radio continuum emission from the disk as well as the halo. NGC 891 is the first galaxy in which the existence of two components to the Z-distribution was recognized, namely, the "thin" and "thick" radio disks (Allen, Baldwin, & Sancisi 1978). In the present paper, the distance to NGC 891 is assumed to be 7.2 Mpc; at this distance, 1′ corresponds to ~2.1 kpc. The edge-on galaxy NGC 4565 is seen at an inclination angle of more than 85°.5, and its radio continuum morphology has also been recognized to consist of both thin and thick components of moderate surface brightness (Broeils & Sancisi 1985). The distance to NGC 4565 is assumed to be 9.4 Mpc; at this distance, 1′ corresponds to ~2.7 kpc.

2. RADIO OBSERVATIONS AND RESULTS

2.1. *NGC 891 at* 6 cm

We observed NGC 891 at 6 cm wavelength with the Very Large Array (VLA)[2] in its "D" configuration during 1988 August for a duration of ~13 hr. The observations were made at two frequency bands centered around 4835 and 4885 MHz, each having a bandwidth of 50 MHz. Since the observations were primarily aimed at detecting linearly polarized emission from the galaxy, special care was taken to observe the unpolarized calibrating source 3C 48 at frequent intervals during its transit. This provided coverage over a wide range of parallactic angles, thereby yielding a good calibration for the instrumental polarization of the antennas. The average residual instrumental polarization after this calibration was found to be less than 0.5%. In addition, the standard polarized calibrating sources 3C 286 and 3C 138 were observed a number of times in order to obtain amplitude and phase calibrations for the total and polarized flux densities, as well as to calibrate the linear polarization reference angles. The data quality was generally good, with a small amount of interference occasionally seen from some of the antennas which were in close proximity to the receiver building. These data were rejected, as were those parts of the observations which suffered from the effects of shadowing of one antenna by another.

The calibrated visibility data at the two adjacent frequency bands were transformed separately using the standard NRAO AIPS software, and intercompared. This proved to be a very valuable check on the internal consistency of the data; in this way, a number of spurious features which appeared on the polarization maps were identified with low-level malfunctions and/or interference in one of the two frequency bands. After removing the offending data, the two frequency bands were combined together.

The final data set contained about a million visibility measurements. This large amount of data, coupled with the necessity to produce maps covering the entire field of view, required considerable computer resources. We have used the CRAY X-MP/48 supercomputer and the MIRIAD reconstruction software package developed for it at the National Center for Supercomputing Applications (NCSA).[3] Maps of size 1024 × 1024 with a 3″ grid separation and an angular resolution of ~12″ were made, and the inner quarter CLEANed down to a level of ~4 times the rms noise as determined from the visibility amplitudes. During the epoch of our observations the radio supernova SN 1986J in NGC 891 was observed nearly at its peak emission at 6 cm (Sukumar & Allen 1989b). This radio supernova served as an excellent "point source" to facilitate the self-calibration of the data using positive CLEAN components. The self-calibration procedure was used to correct for the instrumental *phase variations* alone; the visibility amplitudes were left unchanged. After a few iterations of mapping, CLEANing and self-calibration, the residual phase errors of the antennas were less than 0°.1. The surface brightness sensitivity for structures larger than ~5′ was reduced owing to the absence of antenna spacing less than 40 m. This deficiency was partly alleviated by assuming a zero-spacing total flux density of ~0.36 Jy over the VLA primary beam at 6 cm, including the galaxy NGC 891 (0.29 Jy; Allen et al. 1978) and the supernova SN 1986J (0.07 Jy; Sukumar & Allen 1989b).

The self-calibrated total intensity (I) map was finally CLEANed over an area of ~25′ in the inner quarter, down to a level of about twice the rms noise as estimated from the visibility amplitudes. The data were then similarly analyzed to produce maps for the Stokes parameters Q and U; however, no separate self-calibrations were done for these maps and no zero-spacing flux densities were available. In order to improve the sensitivity to extended regions of polarized emission a small amount of tapering was applied to the visibility data to produce the Q and U maps, which were then CLEANed and restored with a circular beam of 20″. A smoothed map with 20″

[2] The VLA is a facility of the National Radio Astronomy Observatory, which is operated by the Associated Universities Incorporated under agreement with the National Science Foundation.

TABLE 1

OPTICAL PARAMETERS OF NGC 891 AND NGC 4565

Parameter	NGC 891	NGC 4565
Galaxy Type[a]	Sb	Sb
Inclination angle[b]	>88°	>85°.5
Absolute magnitude B_T (mag)[c]	−19.5	−20.4
Radio nucleus position[b]:		
Right ascension (1950)	$02^h19^m24^s.3$	$12^h33^m52^s.06$
Declination (1950)	+42°07′17″.0	+26°15′47″.24
Assumed distance (Mpc)[d]	7.2	9.4
Linear scale (kpc arcmin^{-1})	2.1	2.7

[a] Sandage 1961.
[b] Allen et al. 1978 for NGC 891; Broeils & Sancisi 1985 for NGC 4565.
[c] de Vaucouleurs, de Vaucouleurs, & Corwin 1976.
[d] Based on a Hubble Constant of 100 km s^{-1} Mpc^{-1}.

[3] NCSA is operated by the University of Illinois at Urbana–Champaign with partial support from the National Science Foundation.

resolution was also produced in the total intensity (I). The I, Q, and U maps were then corrected for attenuation by the primary beam (assuming this shape is the same for all Stokes parameters) and used to produce polarized intensity, position angle and percentage polarization maps. The rms noise of the total and polarized intensity maps are ~ 25 and ~ 14 μJy beam^{-1}, respectively.

It may be noted that the effects of the strong background sources 3C 66A and 3C 66B were not seen at 6 cm owing to the smaller HPBW ($\sim 9'$) of the VLA antennas. These sources are situated $\sim 51'$ to the north of NGC 891 and usually dominate the field at wavelengths longer than 20 cm.

The parameters for the observations of NGC 891 are summarized in Table 2.

2.2. *NGC 4565 at* 20 cm

The 20 cm VLA observations of NGC 4565 were carried out between 1988 January and 1988 August in the B, CD, and D configurations over durations of ~ 4, 10.5, and 10.5 hr, respectively. The observations in the B and D configurations were done at two IF bands centered around 1452 and 1502 MHz each having a bandwidth of 25 MHz. However, observations in the CD configuration were limited to only one IF band centered at 1452 MHz since the other band was allocated to a simultaneous observation of NGC 4565 at 90 cm wavelength. The data quality was good in both B and CD configurations, but the D array data suffered from severe interference and a peculiar problem of unknown nature which appeared as a constant signal in the RL and LR correlations of about nine VLA antennas. This problem persisted over the entire observing period independent of the sky position; these data were eliminated. The remaining data were carefully edited for shadowing, low-level interference and cross talk between nearby antennas. About 50% of the RL and LR correlations were finally rejected before construction of the Q and U maps, resulting in some loss of sensitivity and reducing the response to structures with angular sizes larger than $\sim 8'$ (shortest spacing ~ 120 m). However the total intensity (I) map did not suffer as much, and remains sensitive to structures as large as $\sim 25'$ (shortest spacing ~ 40 m).

As with NGC 891, the calibrated data for NGC 4565 at the two nearby frequency bands were transformed separately into preliminary I, Q, and U maps, and intercompared wherever possible. For the final map constructions the data (consisting of ~ 1.4 million visibility measurements) were transferred to the Cray-2 supercomputer at NCSA and further analyzed using the MIRIAD software package. A zero-spacing flux density of ~ 5 Jy was applied to the visibility data for total intensity, accounting for the many strong background sources within the primary beam ($\sim 30'$) of the VLA antennas at 20 cm. Large size maps (2048 × 2048 with 2.″5 grid separation) were made in the total intensity (I) and the inner quarters were CLEANed and restored to an angular resolution of $\sim 7''$ (circular). The data were then self-calibrated using the CLEAN components to correct for any instrumental phase variations. The final rms phase variation is less than 0.°3 in the entire visibility data on NGC 4565.

In order to facilitate the detection of faint extended features in the polarization, and to provide comparison with the 6 cm maps of NGC 891 described earlier, maps in I, Q, and U with a lower resolution of 20″ (circular) were also made from the self-calibrated data by applying a suitable taper to the visibility data in the spatial frequency domain. These maps were not corrected for the primary beam attenuation since the effect over the relevant field of view is negligible for the VLA antennas at 20 cm. The CLEANed I, Q, and U maps were then used to produce polarization intensity, angle, and percentage maps. At the resolution of 20″ the rms noise limits on the total and polarized intensity maps were ~ 50 and ~ 18 μJy beam^{-1} respectively, resulting from residual phase and amplitude errors which could not be corrected any further.

The parameters for the observations of NGC 4565 are summarized in Table 2.

TABLE 2

OBSERVING PARAMETERS FOR NGC 891 AND NGC 4565

Parameter	NGC 891	NGC 4565
Observing wavelength (cm)	6.2	20.3
VLA configurations	D	B, CD, D
Number of antennas used for:		
Total intensity	26	27, 27, 27
Polarized intensity	26	25, 25, 18
Bandwidth (MHz)	100	50, 25,[a] 50
Duration of observations (hr)	13	4, 10.5, 10.5
Zero-spacing flux density (Jy)	0.36	5.0
Restored beam[b]	20″	20″
Map grid spacing	4″	7″
rms noise (μJy beam^{-1}) in:		
Total intensity	25	50
Polarized Intensity	14	18

[a] Only one IF band (AC) used.
[b] Circular, appropriate taper applied to visibilities.

3. OPTICAL IMAGES AND ASTROMETRY

Optical images of NGC 891 and NGC 4565 were provided to us by A. Sandage for comparison with our radio continuum polarization results. These images were taken from plates (PH-208-S and PH-163-MH, respectively) made with the Palomar 200 inch Hale Telescope, and are shown in the Hubble Atlas (Sandage 1961; see Atlas, p. 25).

The radio contour maps described in this paper have been positioned on the optical images using a number of stellar objects in the field as points of reference. The positions of these objects (which have otherwise been selected arbitrarily) have been measured in the reference frame of the first Guide Star Catalog (GSC-I; Lasker et al. 1990) using the Guide Star Astrometric Package at the Space Telescope Science Institute (ST ScI). The images of NGC 891 and NGC 4565 used for this purpose were electronically retrieved from the digitized versions of the appropriate Palomar "Quick-V" survey plates which are stored at ST ScI, and the objects chosen visually on a computer display screen. The objects are marked with crosses in many of the figures in this paper. Their positions are listed for future reference in Table 3.

4. ANALYSIS OF THE RESULTS

The highest resolution total intensity maps available from our observations (12″ for NGC 891 at 6 cm, and 7″ for NGC 4565 at 20 cm) will be presented and discussed elsewhere. The polarization images, which are the main subject of the present paper, have been reconstructed to a resolution of 20″ (circular FWHM) in order to enhance the sensitivity to faint extended features. The total intensity maps presented here have therefore been smoothed to the same resolution for comparison.

TABLE 3

POSITION OF STELLAR OBJECTS IN THE FIELDS OF NGC 891 AND NGC 4565 (Epoch 1950)

Right Ascension	Declination	Notes
$02^h19^m09^s.64$	42°02′03″.1	
02 19 11.82	42 02 26.0	
02 19 12.23	42 11 05.3	a
02 19 12.94	42 10 08.6	a, b
02 19 14.27	42 02 31.2	
02 19 15.35	42 01 37.1	a
02 19 15.81	42 03 20.2	c
02 19 18.85	42 08 23.6	a
02 19 28.47	42 11 30.5	a, d
02 19 30.05	42 06 03.5	a
02 19 38.51	42 10 06.1	e
02 19 40.98	42 08 28.1	a
12 33 32.91	26 17 44.2	
12 33 40.02	26 14 57.6	
12 33 44.00	26 12 20.2	a
12 33 48.25	26 20 24.7	
12 33 56.28	26 22 09.6	
12 33 56.65	26 16 51.5	a
12 34 15.79	26 12 20.2	

[a] Object position from version 1 of the Guide Star Catalog.

[b] Too bright; not plotted on contour maps.

[c] Confused, in disk of NGC 891; non-stellar?; plotted but not used.

[d] Confused; two fainter stars nearby.

[e] Too faint; plotted but not used.

4.1. *NGC 891 at 6 cm*

The total (I) and polarized (P) radio continuum surface brightnesses of NGC 891 at 6 cm wavelength are shown in Figures 1*a* and 1*b* (Plates 9 and 10) at a resolution of 20″ as intensity contours following a power law $2^{N/2}$ where $N = 1, 2, 3 \ldots$ etc. In both Figures 1*a* and 1*b* the map contours are superposed with line segments ("E vectors") whose lengths are proportional to the magnitude of P and whose orientations indicate the direction of maximum linear polarization. Figure 1*c* (Plate 11) shows the percentage of polarized emission ($100 \times P/I$) as contours starting at 2% and increasing in a power law of 2^N where $N = 1, 2, 3 \ldots$ etc.

The total intensity map of NGC 891 at 6 cm in Figure 1*a* bears a striking resemblance to the 20 cm map first published by Allen et al. (1978), except for the presence of SN 1986J ~1′ southwest of the nucleus of the galaxy. The great similarity of the I maps at these two widely spaced wavelengths qualitatively confirms the general constancy of the radio spectral index over much of the galaxy image, as first reported by Allen & Hu (1985). The regular spacing of the logarithmic contour levels in Figure 1*a* indicates an approximately-exponential decrease of surface brightness at 6 cm with increasing distance from the plane of the galaxy. A correlation of the optical and 20 cm radio continuum surface brightnesses at faint levels in NGC 891 has been reported by Hu et al. (1987; see also Allen et al. 1990). The radio continuum spectral index distribution and the relation between the radio continuum and optical continuum surface brightnesses will be discussed in future papers; for the present, we wish to concentrate on the appearance and interpretation of the polarization maps in Figures 1*b* and 1*c*. Five features are indicated with labels on the polarized surface brightness map of Figure 1*b*. F_1 and F_2 lie on opposite sides of the major axis of NGC 891 ~2′ to the north of the nucleus; features B_1 and B_2 are roughly in the same position but to the south of the nucleus. The peaks of features F_2 and B_2 are located ~20″ away from the plane of the galaxy to the east. Features F_1 and B_1 peak up a little further away from the plane to the west, at ~30″. A ridge R_1 of polarized emission extends from feature F_1 to feature B_1; this ridge runs parallel to the major axis, ~30″ to the west. Feature F_3 is the brightest component on Figure 1*b*. Its peak lies 53″ from the nucleus in a northerly direction along the major axis, and ~6″ off the plane in Z to the west. It is elongated by ~90″ in P.A. + 4°. There is no counterpart to F_3 on the southern side.

The position angle of the maximum polarization (the "E-vectors" in Figs. 1*a* and 1*b*) intrinsic to the image of NGC 891 depends on the amount of Faraday rotation suffered by the radio emission as it traverses the intervening material in our own Galaxy. The amount of Galactic foreground rotation is not known with certainty in the direction of NGC 891; it is tentatively estimated to be -72 ± 3 rad m^{-2} (E. Hummel, private communication). In that case, foreground Faraday rotation would amount to less than 15° at 6 cm, and the E-vectors drawn on Figures 1*a* and 1*b* represent very nearly the intrinsic directions of maximum polarization over the image of NGC 891.

4.2. *NGC 4565 at* 20 cm

The intensities of the total and polarized radio continuum emission from NGC 4565 along with the percentage of polarized emission at 20 cm wavelength are shown as contours in Figure 2*a*–2*c* (Plates 12–14) with levels similar to Figures 1*a*–1*c*. The brightness distribution of total intensity (Fig. 2*a*) is noticeably thinner than that of NGC 891. At first sight, the polarized radio emission from NGC 4565 in Figure 2*b* is quite different from that of NGC 891 in Figure 1*c*. Most striking is the fact that the polarized emission from NGC 4565 appears essentially only on the southeast side of the nucleus; it virtually disappears on the northwest side. The polarized emission is found in two elongated structures, placed roughly symmetrically in Z on either side of the galactic disk, and strongest at ~1′ (3 kpc) to the southeast of the nucleus. These features are labeled F_1 and F_2 on Figure 2*b*. In this respect the polarized emission of NGC 4565 bears some resemblance to that of NGC 891, although it is not as bright. The distance of this emission from the galactic plane in NGC 4565 seems to increase slightly, from ~1.5 kpc near the center of the galaxy to ~2 kpc at a radius of 7.5 kpc.

The line segments on Figure 2*b* are oriented everywhere almost perpendicular to the galactic disk. The foreground Faraday rotation by the Galaxy is expected to be very small for this general direction in the sky; the rotation measure for NGC 4631 (which is only ~6° away from NGC 4565) is estimated from observations of the rotation measures of background sources within 10° to be -6 ± 6 rads m^{-2} (Hummel et al. 1988). The line segments on Figure 1*b* are therefore a good indication of the direction of maximum polarization of the emission emerging from the galaxy itself. The Faraday rotation internal to NGC 4565 is not known, and may be more severe at 20 cm than was expected in the case of NGC 891 at 6 cm. However, we will argue in § 5 below that the polarization seen on the east side of NGC 4565 is coming mostly from the *front edge* of the galaxy. In that case there is very little internal Faraday rotation; the line segments on Figure 1 then show that the magnetic field in NGC 4565 is generally parallel to the plane, as it was in NGC 891.

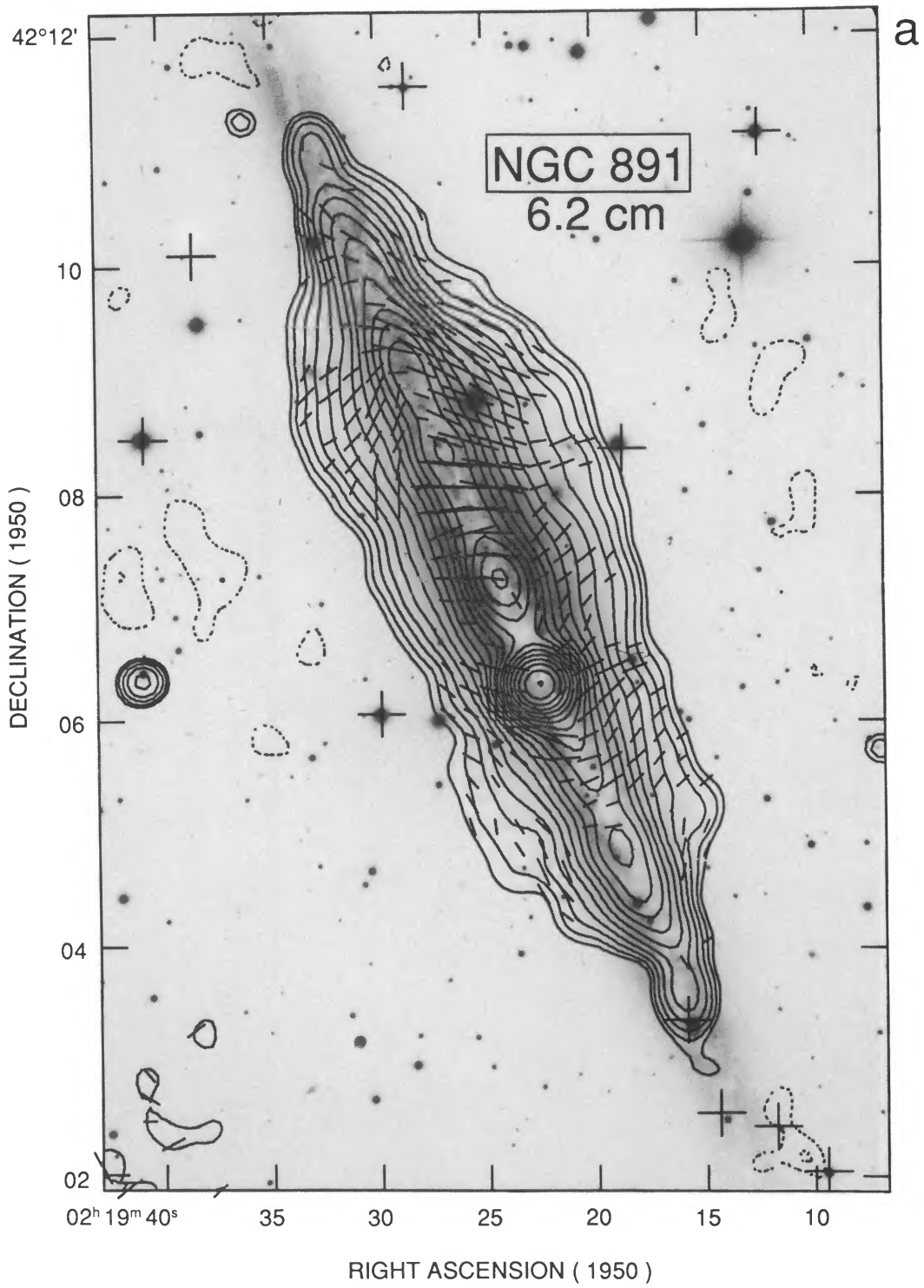

FIG. 1*a*

FIG. 1.—(*a–b*) Contours of the total (linearly polarized) radio continuum surface brightness at 6 cm from NGC 891. Contours start at 150 μJy beam^{-1} (70 μJy beam^{-1}) and increase by $2^{N/2}$. Negative contours are dotted. The line segments drawn over these contour maps have lengths proportional to the linearly polarized surface brightness at their centers with 1″ on the plot equivalent to 8.33 μJy beam^{-1}; the direction of a segment indicates the position angle of maximum polarization. Segments have not been plotted if the total intensity is less than 150 μJy beam^{-1} or the polarized intensity is less than 70 μJy beam^{-1}. The restoring beam width is 20″ circular FWHM for both maps. A correction for attenuation of the primary beam has been applied. The rms noise near the center of the field is $\sim$25 (14) μJy beam^{-1}. SN 1986J is the bright point source in the galaxy disk in Figure 1*a*, $\sim$1′ southwest of the nucleus. In (*c*) the percentage of linearly polarized radio emission is shown in contours, increasing as 2^N starting at 2%; contours are not plotted if the total intensity is less than 150 μJy beam^{-1} or the polarized intensity is less than 70 μJy beam^{-1}. The underlying optical images have been provided by A. Sandage.

PLATE 10

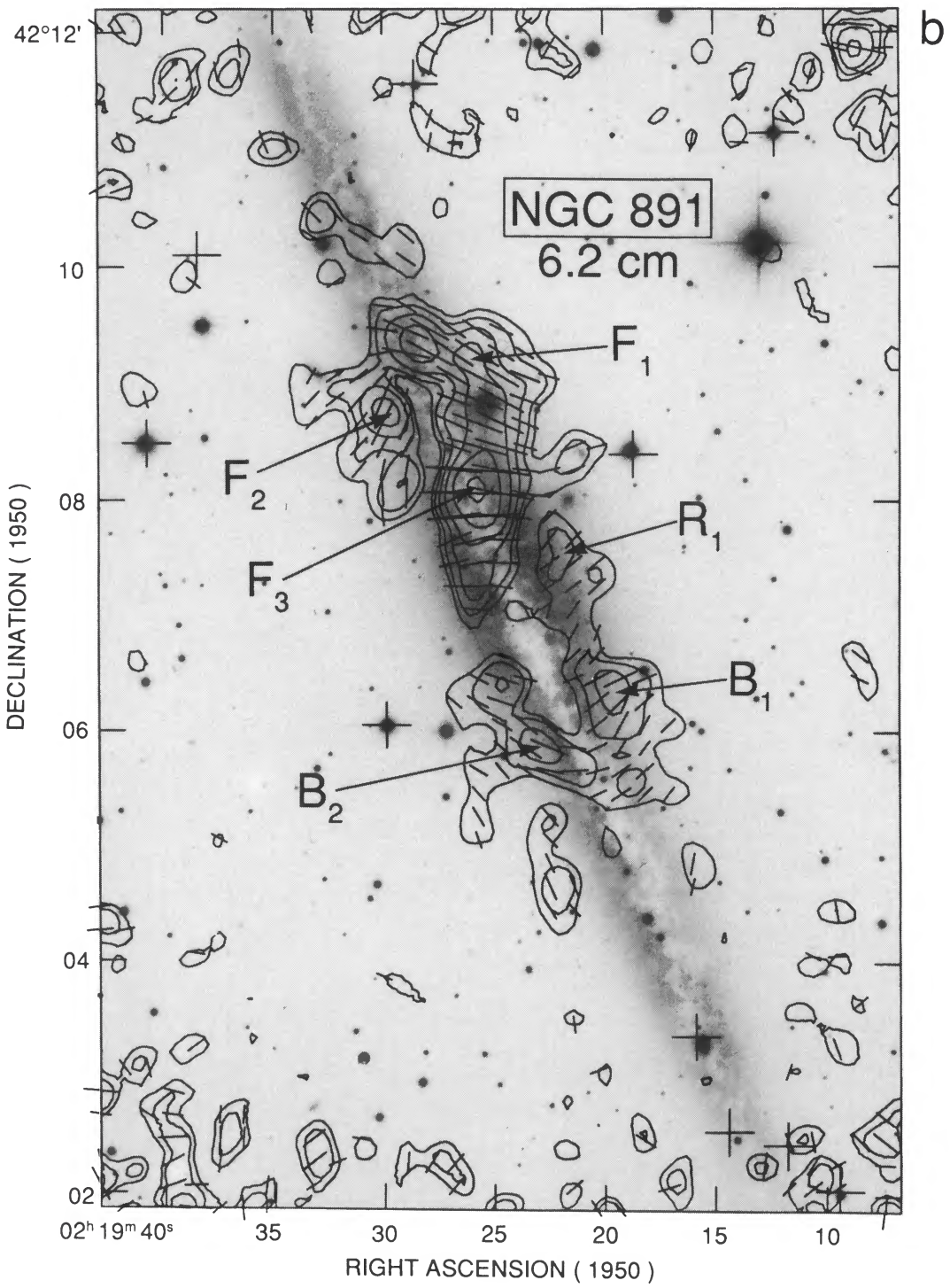

FIG. 1*b*

SUKUMAR & ALLEN (see 382, 103)

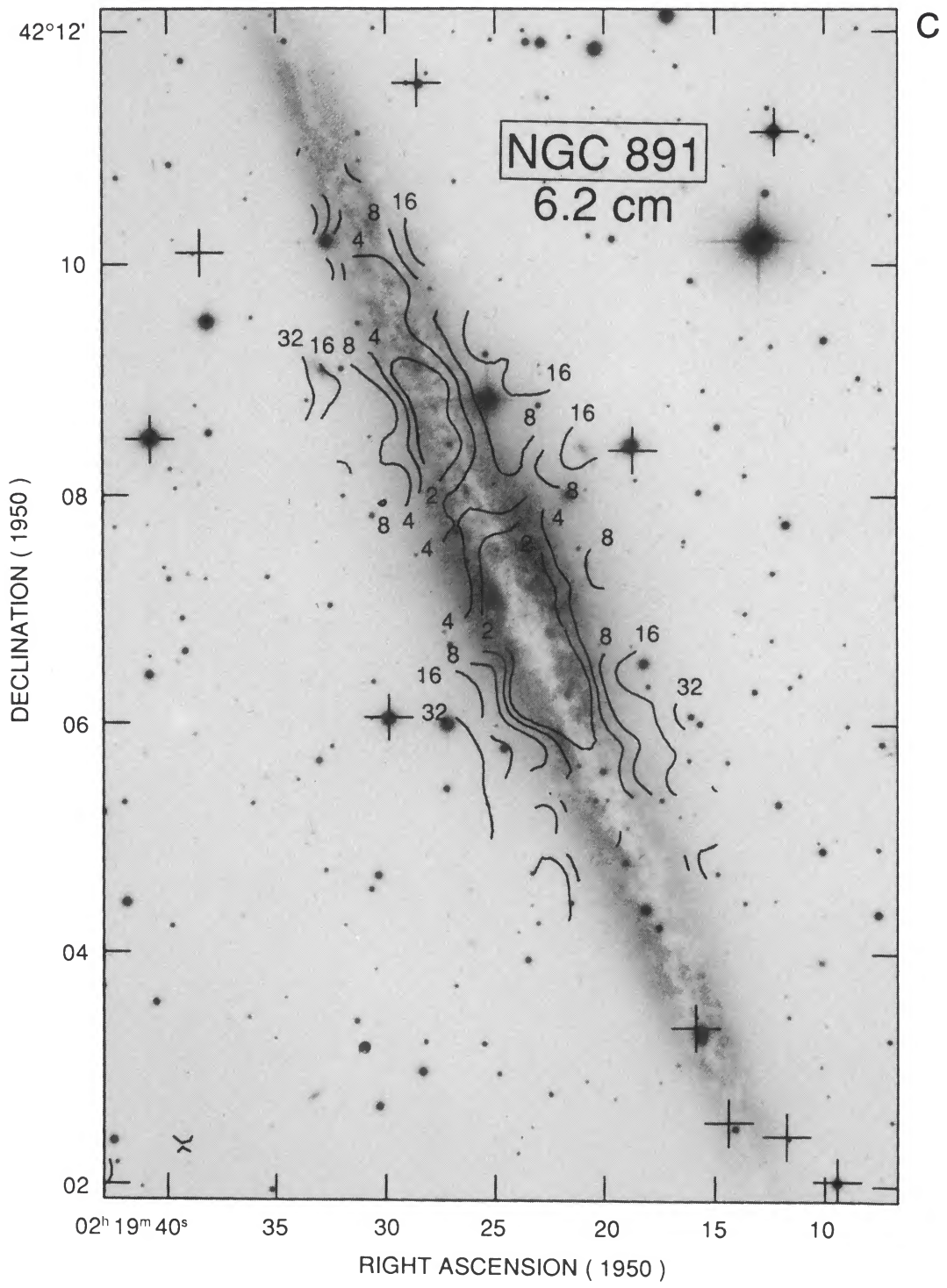

FIG. 1c

SUKUMAR & ALLEN (see 382, 103)

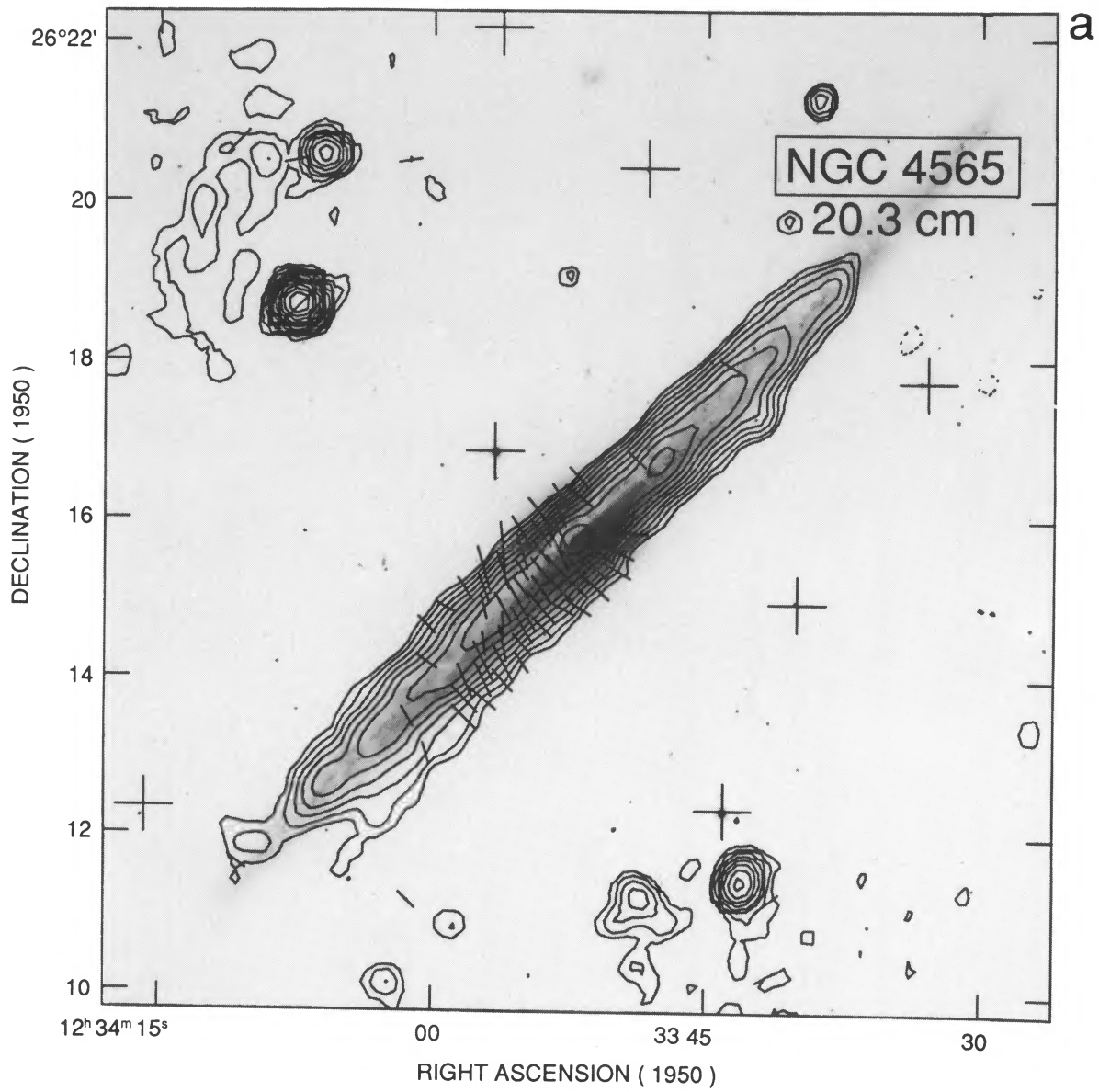

FIG. 2*a*

FIG. 2.—(*a–b*) Contours of the total (linearly polarized) radio continuum surface brightness at 20 cm from NGC 4565. The contours start at 200 μJy beam^{-1} (70 μJy beam $^{-1}$) and increase by $2^{N/2}$. Negative contours are dotted. The line segments drawn over these contour maps have lengths proportional to the linearly polarized surface brightness at their centers with 1″ on the plot equivalent to 4.76 μJy beam^{-1}; the direction of a segment indicates the position angle of maximum polarization. Segments have not been plotted if the total intensity is less than 200 μJy beam^{-1} or the polarized intensity is less than 80 μJy beam^{-1}. The restoring beam width is 20″ circular FWHM for both maps and the rms noise is $\sim$50 (18) μJy beam^{-1}. A correction for the VLA primary beam is negligible at 20 cm and has not been applied. In (*c*) the percentage of linearly polarized radio emission is shown as contours increasing as 2^N starting at 2%; contours are not plotted if the total intensity is less than 200 μJy beam^{-1} or the polarized intensity is less than 70 μJy beam^{-1}. The underlying optical images have been provided by A. Sandage.

SUKUMAR & ALLEN (see 382, 103)

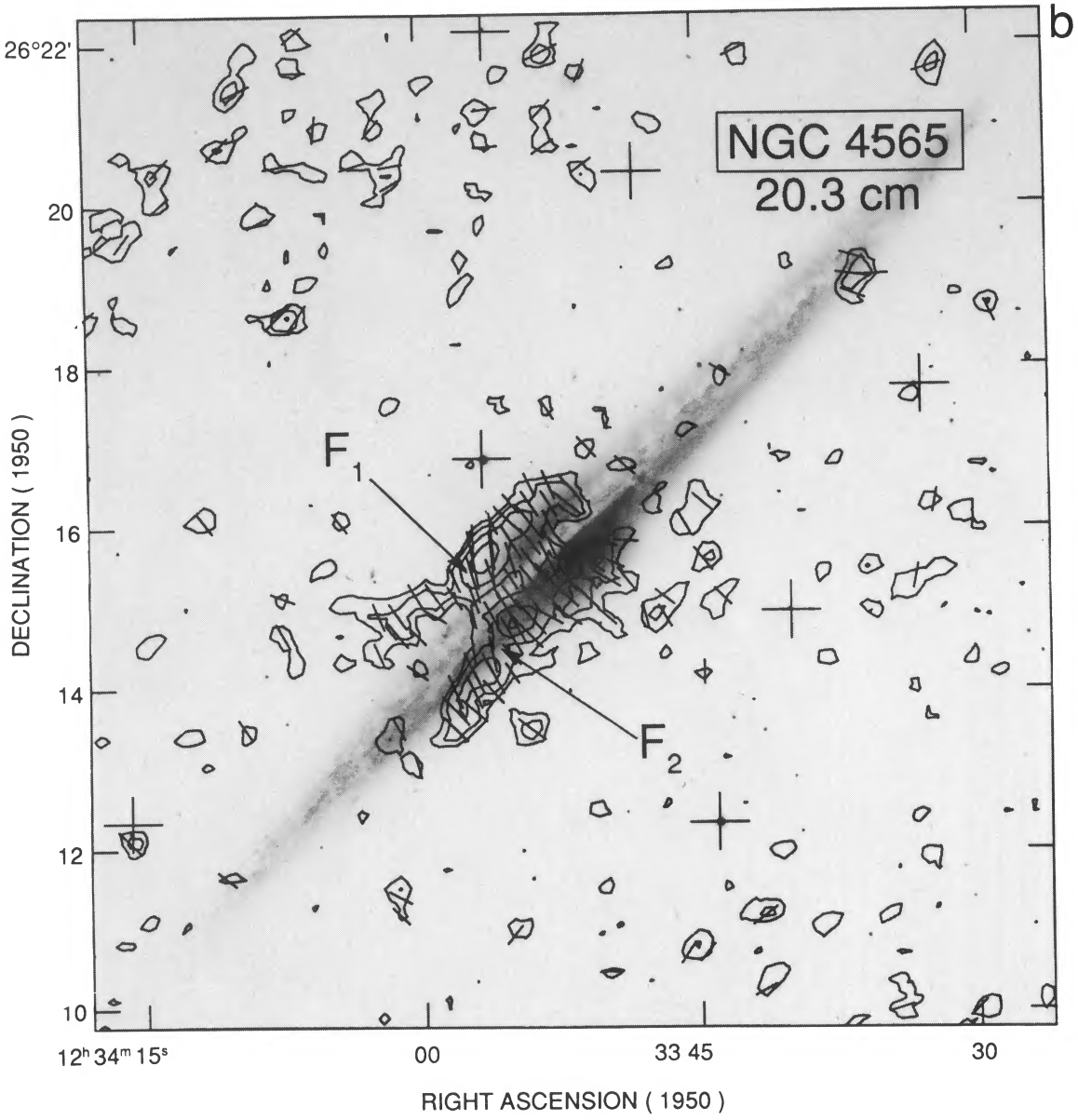

FIG. 2*b*

SUKUMAR & ALLEN (see 382, 103)

PLATE 14

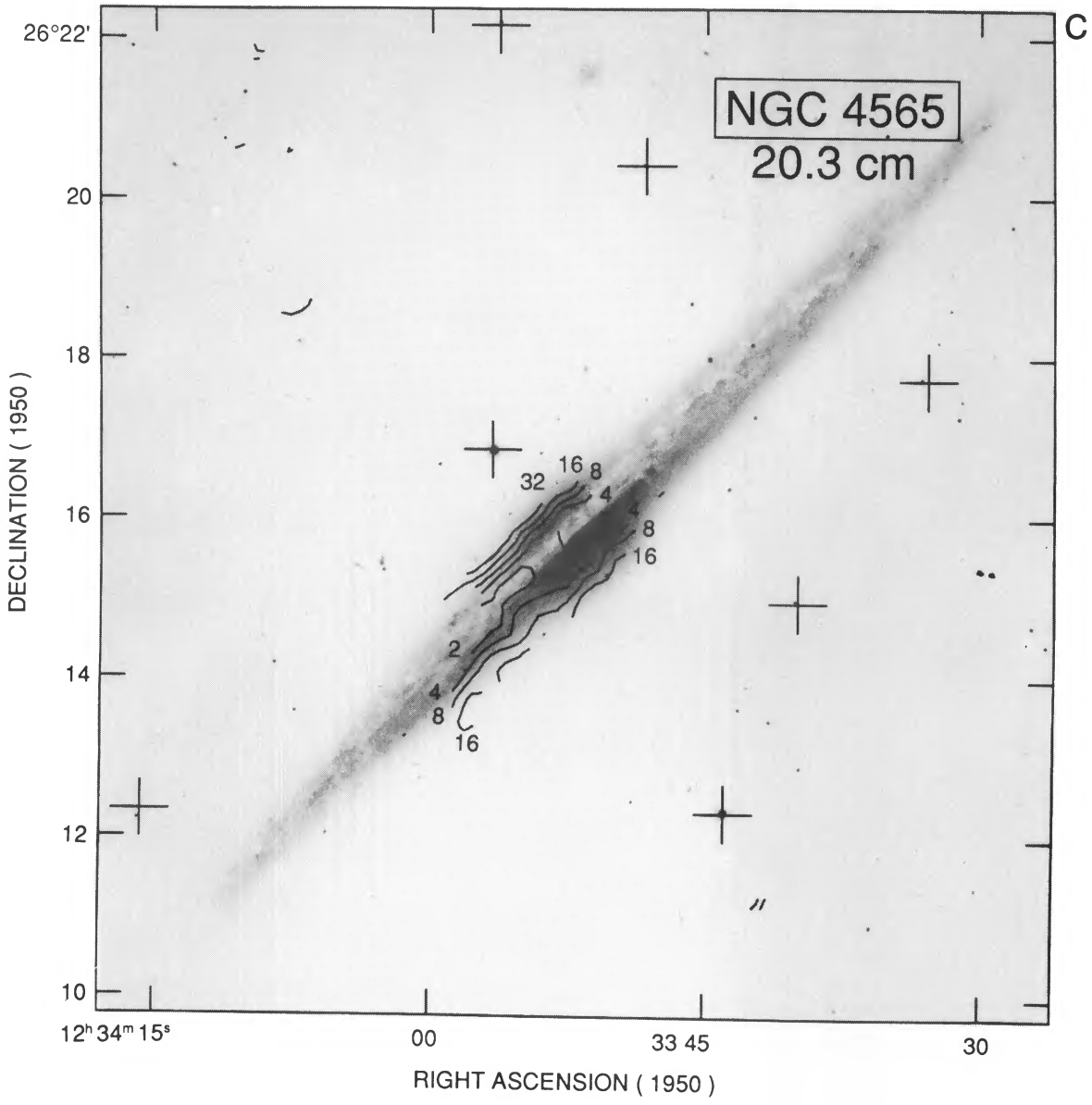

FIG. 2*c*

SUKUMAR & ALLEN (see 382, 103)

5. DISCUSSION: TOWARD A UNIFIED MODEL

The major features we seek to model are the following:

1. The distribution of 20 cm polarization shows a striking asymmetry about the minor axis of NGC 4565, being virtually absent on the west side, whereas a high degree of symmetry appears in the 6 cm image of NGC 891.

2. The degree of polarization is less than a few percent in the plane of both galaxies at $Z = 0$, but increases rapidly with distance above the plane, reaching over 30% in NGC 891 at a Z-distance of 2 kpc.

Can we understand these observed features of the polarization in edge-on galaxies in terms of a single three-dimensional model of the distribution of ordered and disordered magnetic field in normal disk galaxies?

When observed with sufficient resolution to separate spiral arm from interarm emission, normal *face-on* galaxies generally show polarization which is strongest in the dark interarm and outer regions of the disks. We have reported earlier on this feature of the polarized radio emission from M83 (Sukumar & Allen 1989a), and it has also been recognized in recent observations of M51 (Horellou et al. 1990) and M81 (Krause et al. 1989). In M83 for example, the strongest linearly polarized emission is found in two giant arcs, with typical lengths of ~ 30 kpc, which are situated roughly opposite each other at a radius of 12 kpc from the center of the galaxy. These regions of high polarized intensity (and thus of highly uniform magnetic field) do not coincide with any prominent spiral arm tracers. Our explanation for this phenomenon (Sukumar & Allen 1989a) is that turbulence associated with the star formation process tangles the magnetic field on the scale of 100 pc or so, and it is only in the more quiescent interarm and outer regions of the disk where the magnetic field is able to retain a large-scale order.

At first sight, the distributions of polarized emission for the two edge-on galaxies described in the present paper would appear to present yet another new puzzle. However, they do share at least one common trait with the face-on systems: The regions of strongest polarization are found in those parts of the galaxy which are removed from the sites of active star formation. For the edge-on systems, these regions are located well above the galactic plane. We may therefore expect that the low polarization near $Z = 0$ is also related to turbulence in the interstellar medium associated with the star formation process. Nevertheless, this activity clearly cannot explain the appearance of asymmetry in the distribution of polarization on either side of the minor axis in NGC 4565 at 20 cm.

A feature of galaxies viewed edge-on which clearly differs from those viewed face-on is the much greater path length through the interstellar gas. Emission located on the far edge of the galaxy may be severely affected by Faraday depolarization (Burn 1966), whereas emission from the near edge would be largely unaffected. Modeling the observed morphology of the polarized emission requires information about the geometry of the polarized regions, the structure of the magnetic field, and the amount and distribution of ionized gas.

5.1. *A Three-dimensional Model*

Our model galaxy is patterned after our observations of M83 (Sukumar & Allen 1989a, 1990), with the addition of an assumed thickness in Z. In Figures 3*a* and 3*b* we reproduce the observed results on M83 for reference. The model, which is a simplified version of Figure 3*b*, has two 90° arcs of ordered magnetic field in opposite quadrants of the disk at a radius of 12 kpc from the center. The arcs have a radial thickness of ~ 1 kpc, and are assumed to have the same extent in Z as the total emission (~ 2 kpc on either side of the disk). The variation of polarization with Z in the arcs will be discussed later. The central disk of the galaxy is filled with synchrotron-emitting material, as in Figure 3*a*; the magnetic field in this region is

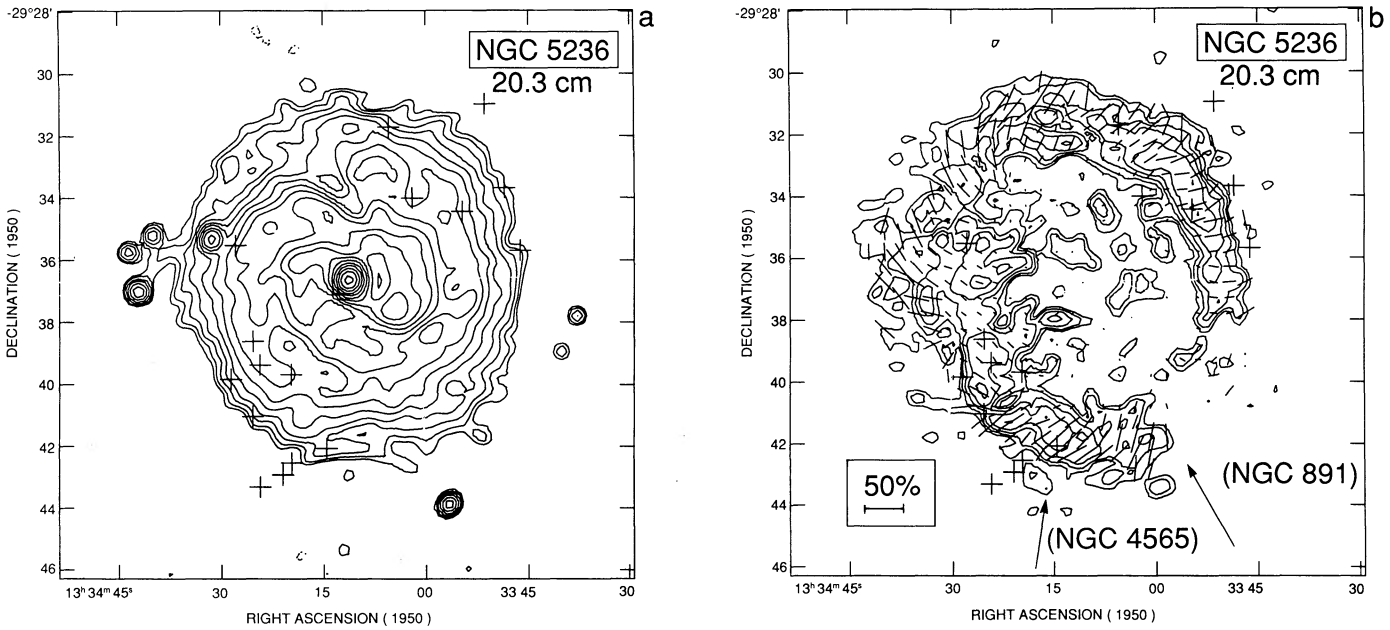

FIG. 3.—(*a–b*) Distribution of total (linearly polarized) 20 cm radio continuum surface brightness of M83, from Sukumar & Allen (1990). Contours start at 0.6 mJy beam^{-1} (0.15 mJy beam^{-1}) and increase by $2^{N/2}$. The resolution is 30″. This is essentially the face-on view of our model for NGC 891 and NGC 4565; the viewing direction is indicated for two cases intended to approximate the situation for these two edge-on galaxies.

evidently tangled on the scale of ~ 100 pc or less, so that the intrinsic degree of polarization is very low.

The central disk in our model galaxy is also filled with ionized gas. The distribution of this ionized gas is based on the observational results of Rand et al. (1990), who used narrow-band imaging of the Hα and [S II] emission lines to map the warm interstellar medium in NGC 891. Those authors have modeled the observed Hα emission measure in NGC 891 with a relation for the volume density of thermal electrons of the form:

$$n_e(R, Z) = \langle n_e^0 \sqrt{\phi/0.25} \rangle \exp(-|Z|/Z_0) \exp(-R/R_0); \quad (1)$$

where $\langle n_e^0 \rangle$ is the rms thermal electron density at $R = Z = 0$, ϕ is the filling factor (assumed everywhere the same), and R_0 and Z_0 are the scale lengths in R, and Z respectively. Rand et al. fitted a three-component model to the north and south sides of the galaxy separately, including "Bulge," "Disk," and "Halo" components on each side. We have constructed an average model from their results and adjusted the parameters for our assumed distance of 7.2 Mpc to NGC 891. In Table 4 we summarize the parameters of the ionized gas distribution in our model, which we take to apply both to NGC 891 and to NGC 4565.

5.2. *Effects of Faraday Depolarization*

Burn (1966) has considered many aspects of the depolarization of centimeter radio synchrotron radiation. The presence of the interstellar magnetic field and ionized gas leads to a "Faraday rotation" $\Phi = \mathrm{RM}\lambda^2$ (rads) of the plane of polarization of the radio emission (see, e.g., Burn 1966, eq. [2]), where the rotation measure RM is

$$\mathrm{RM} = 0.81 \int n_e H_{\parallel} \, dl \,, \quad (2)$$

in units of radians m^{-2}, where n_e is the electron density in cm^{-3}, $H_{\parallel}$ is the line-of-sight component (with corresponding sign) of the magnetic field in micro Gauss, and distance l along the line of sight is measured in parsecs.

The magnetic field is likely to have many sign reversals along the line of sight as the radiation traverses the interstellar medium. A typical scale length for these reversals may be ~ 100 pc (see for example the discussion referenced in Ruzmaikin et al. 1988, p. 148). The net result will be only a small amount of rotation of the plane of polarization along any given line of sight to emission situated on the far side of the galaxy, but there will be a significant decrease in the *amount* of polarization with increasing wavelength as a consequence of vector-summing "scrambled" polarization vectors for each line of sight in the observing beam. The emergent polarization (p) is related to the initial polarization (p_i) according to (Burn 1966, eq. [21]):

$$p \approx p_i \exp[-2\mathrm{RM}^2_{\mathrm{random}}(L/l)\lambda^4] \,. \quad (3)$$

TABLE 4

DISTRIBUTION OF WARM INTERSTELLAR MEDIUM IN OUR MODEL GALAXY[a]

Component	$n_e^0\sqrt{\phi/0.25}$ (cm^{-3})	Z_0 (kpc)	R_0 (kpc)
"Bulge"	0.15	1	2.5
"Disk"	0.10	0.6	6.5
"Halo"	0.03	2	9

[a] Adapted from the observations of NGC 891 by Rand, Kulkarni, & Hester 1990.

Note the strong dependence on wavelength in this equation. As an example, the electron density n_e for the model galaxy in Table 4 is ~ 0.03 cm^{-3} at a Z-distance of 1 kpc. For a total foreground path length $L \sim 10$ kpc, reversal scale length $l \sim 100$ pc, and random field strength $H_{\parallel} \sim 1$ μG we find $\mathrm{RM}_{\mathrm{random}} \sim 2.4$ rad m^{-2}. At 20 cm wavelength, the average intrinsic polarization of a region lying at the far end of the line of sight will be reduced by a factor ~ 7, whereas at 6 cm the reduction is only $\sim 2\%$.

For a more quantitative example, we have computed the observed projected two-dimensional distribution of polarization from our three-dimensional model, assuming the strength of the random magnetic field to be 1 μG everywhere. Figure 4 shows the polarized surface brightness of NGC 4565 as a function of radius from the center of the galaxy. The 20 cm data (*solid lines*) from both sides of the plane have been averaged in strips of 0.3×3.8 kpc wide parallel to the minor axis, excluding the range in Z near the galactic plane from -0.6 kpc to $+0.6$ kpc. The crosses show the polarization from the model galaxy at 20 cm wavelength, scaled in amplitude and averaged over similar strips to correspond approximately to the observations. The emission east of the minor axis is on the near side of the galaxy and has hardly been affected by Faraday depolarization, whereas the emission west of the minor axis comes from the far side of the galaxy and has been almost entirely depolarized. The slight extension of the polarized emission across the minor axis is accounted for by an appropriate choice of viewing angle, as shown in Figure 3*b*. A plot from model calculations at 6 cm is superfluous, being nearly symmetric at an approximately constant level about the minor axis; this agrees with the observations of NGC 891.

There are two obvious predictions which can be made in the framework of our model. First, we predict that polarized emission will be observed on the west side of the minor axis of NGC 4565 at short centimeter wavelengths (e.g., 6 or 2 cm), as features appear which are located on the far side of the galaxy and which are presently obliterated at 20 cm by Faraday depolarization. Second, NGC 891 will become much more asymmetric at decimeter and longer wavelengths (e.g., 20 or 50 cm) as the

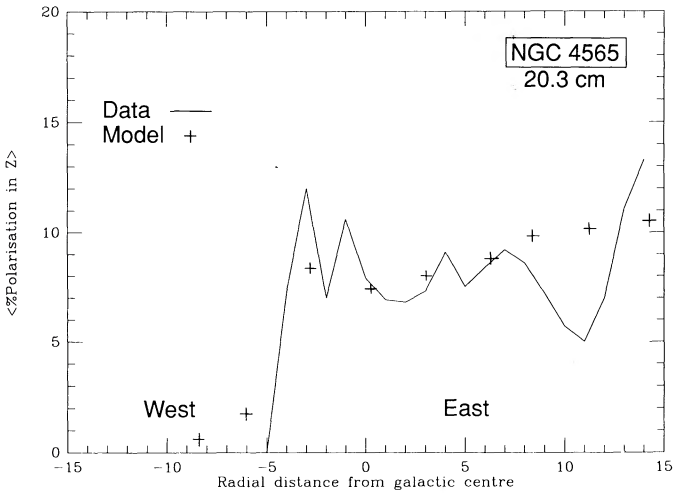

FIG. 4.—Polarized surface brightness in NGC 4565 at 20 cm as a function of radial distance from the center of the galaxy (*solid line*). One unit of distance on the X-axis is $7'' \sim 300$ pc. The crosses are the values computed every $20'' \sim 900$ pc for the model galaxy seen edge-on. See text for a description of the averaging procedure used.

"background" features B_1 and B_2 disappear behind a depolarizing Faraday screen. Our choice of "foreground" and "background" features in the case of NGC 891 is based on details of the observed polarization which will be discussed in the next section.

The strong dependence on wavelength in equation (3) provides another method for estimating the line-of-sight–averaged magnetic field strength. Maps of the fractional polarization are required at the same angular resolution for several radio wavelengths spanning the range where the galaxy rapidly becomes optically thick. Using equation (3), one can then construct a map of the distribution of $\mathrm{RM}^2_{\mathrm{random}}(L/l)$. Optical images of emission-line intensities smoothed to the same resolution provide estimates of the mean square column density of electrons. Using this in the previous equation then allows computation of a map of $H_{\|}$ averaged along the line of sight. Assumptions about the electron density filling factor, the total foreground path length through the galaxy to the polarized arcs, and the scale size of the magnetic field reversals are still required.

We note finally that we have not included any possible effects of "internal" Faraday depolarization, arising as a result of the presence of thermal plasma embedded in the arcshaped polarized regions where the magnetic field is apparently ordered on the scale of several kiloparsecs. We can again use the results of Burn (1966) to estimate the depolarization in the simple model of a uniform slab of synchrotron-emitting gas with a constant magnetic field. The polarization for this case follows a $\sin\Phi/\Phi$ dependence with $\Phi = \mathrm{RM}\lambda^2$. In our model, the slab is $\sim$2–3 kpc thick, leading to a reduction at 20 cm wavelength of the intrinsic $\sim$75% polarization by a factor of $\sim$2–3 for an ordered magnetic field component along the line of sight of $H_{\|} \sim 1$ μG and a thermal electron density of 0.03 cm^{-3}. While this at first sight appears consistent with the observed levels of $\sim$20–30% polarization at high Z in NGC 4565 at 20 cm, this type of depolarization is accompanied by a rapid change in the position angle Φ of maximum polarization as the electron density changes with position over the image of the galaxy. However, the observations in Figure 2 show very little change in Φ with position. We conclude that this type of internal Faraday depolarization is not significant. Since there is little doubt that the ionized gas and ordered fields are both present in the general area of the polarized arcs, the uniform slab model must be an oversimplification; there is apparently considerable additional substructure in the synchrotron-emitting regions. This is in agreement with more detailed observations of the polarization structure of M83 at 20 cm which shows the polarized arcs breaking up into smaller, highly polarized "granules" (Allen & Sukumar 1990). The path lengths through these granules will be shorter, and since they are located away from the sites of the most active star formation, the local density of ionized gas may also be reduced. Both of these effects will reduce the amount of internal Faraday depolarization.

5.3. *Z-Distribution of Polarization*

While Faraday depolarization in a turbulent intervening medium offers a reasonable explanation for the observed asymmetry of the polarized emission about the minor axis in NGC 4565 at 20 cm (and the symmetry of NGC 891 at 6 cm), it does not provide an explanation for the decrease in the degree of polarization at low Z in both galaxies as shown in Figures 1*c* and 2*c*. At 20 cm, the polarized arc which we see at the east side of NGC 4565 in Figure 2 is on the *front edge* of the galaxy disk; the Faraday depolarization will be small there since the path lengths through the foreground medium in the galaxy are expected to be small. In the framework of our model, there is virtually no Faraday depolarization anywhere in NGC 891 at 6 cm with the possible exception of a narrow band within a few hundred parsecs of the plane. In our interpretation, Figure 1*c* therefore represents very nearly the intrinsic distribution of polarization.

Since it is unlikely that the decrease in polarization at low Z is a propagation effect, it must be intrinsic to the mechanism by which the polarized emission is formed, i.e., it must be a local effect. Local disordering of the magnetic field would reduce the polarization, and could be caused by a number of processes such as star formation, various magnetic field instabilities which may lift and twist field lines out of the plane, and so on. Burn shows (1966, eq. [10]) that the polarization p_0 of $\sim$75% which is characteristic of synchrotron emission in a completely ordered magnetic field is reduced by the ratio of the energy in the uniform field ($\boldsymbol{B}$) to the energy in the total field ($\boldsymbol{H}$) in the approximation that the radio spectral index is 1 (to which the expression is not sensitive). In the present case, we must modify this result by the ratio of the path length $d(Z)$ through the polarized arc to the path length D for the total emission (essentially the diameter of the galaxy), so that:

$$p(Z) \approx p_0(B_{\perp}^2/H_{\perp}^2)[d(Z)/D] \, . \tag{4}$$

In Figure 5 we have plotted the average percentage polarization in NGC 891 as a function of Z, as detemined from our 6 cm observations. The data have been averaged in narrow strips 1′ in length oriented parallel to the major axis; the resolution remains 20″ in the Z-direction. Figure 5*a* shows the results for the strips centered at 1.′5 and 0.′5 to the northeast (the "foreground" side of the galaxy), and Figure 5*b* the results for the strips at 0.′5 and 1.′5 to the southwest (the "background" side). In our model, these graphs are plots of the Z-dependence of the percentage polarization as given in equation (4).

We can now provide the explanation for why we have designated the polarized features on the southwest side of NGC 891 to be in the "background" instead of those on the northeast side. Figure 5 shows that the fractional polarization near $Z = 0$ is slightly lower for the strip averages on the soutwest side; the effect is strongest in the strip positioned at 0.′5 to the southwest. This is expected if, besides the dominant effect of reducing the polarization by turbulence in the interstellar medium as mentioned above, there is an additional residual Faraday depolarization at 6 cm near $Z = 0$. In fact, using the parameters for the electron density and magnetic field from the last section, and taking account of the slight tilt of the galaxy away from perfectly edge-on, our model predicts a further reduction in the polarization at $Z = 0$ by about a factor of 2 if we assume the polarized features on the southwest side of the galaxy to be at the far edge of the disk.

6. CONCLUSIONS

We have presented maps of the distribution of intensity and linear polarization of the two edge-on galaxies NGC 891 at 6 cm and NGC 4565 at 20 cm wavelength with a resolution of 20″. The major features of the polarization distributions in both galaxies have been explained with a model pattern after the observed polarization features of several nearby face-on galaxies, combined with the effects of Faraday depolarization. We conclude that the appearance of the polarization distribu-

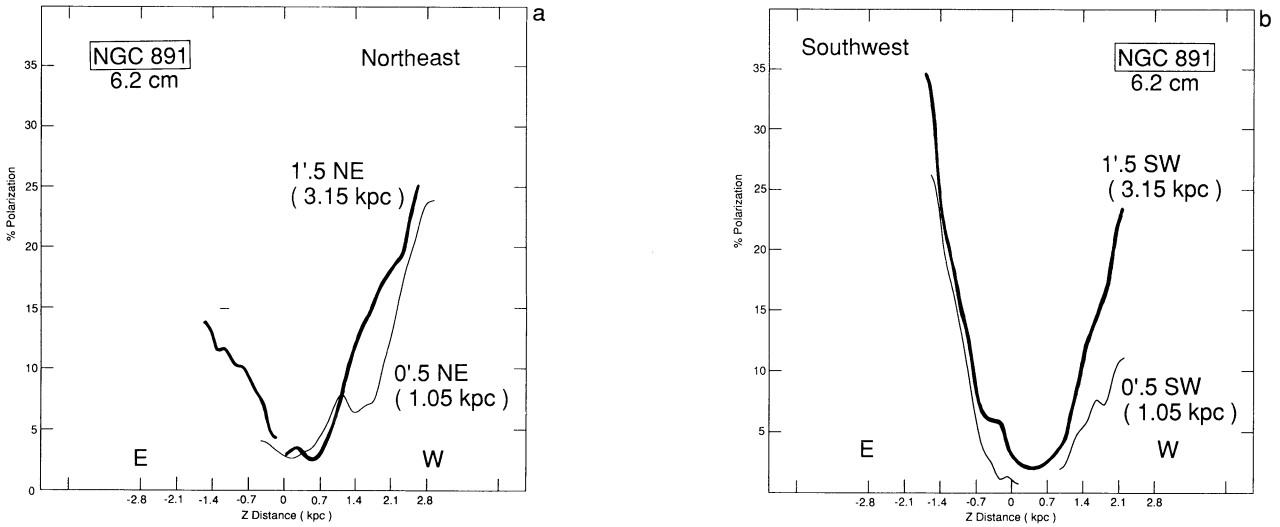

FIG. 5.—Z-distribution of the observed percentage polarization in NGC 891 at 6 cm wavelength. See text for a description of the strip-averaging procedure. (*a*) Data for distances of 0'.5 and 1'.5 to the northeast of the galaxy center. (*b*) Data for 0'.5 and 1'.5 to the southwest. In the model discussed in the text, the emission in (*b*) (especially the curve labeled 0'.5 SW) originates on the far side of the galaxy.

tions of normal disk galaxies viewed edge-on at decimeter wavelengths is severely affected by Faraday depolarization. The importance of Faraday depolarization in this case is a consequence of the long path lengths through the magnetized interstellar medium; it does not require extreme values either for the magnetic field strength or for the electron density.

Faraday depolarization is strongly dependent on wavelength. As a test of our model, we have made specific predictions of changes which we expect to see in the appearance of the polarized emission in NGC 891 and NGC 4565 at radio wavelengths other than those employed for the present observations.[4] We have also pointed out that, with more extensive observations, the methods used in this paper can be inverted to provide a new diagnostic tool for measuring the distribution, degree of order, and strength of magnetic fields in galaxies.

[4] While this paper was being finalized, we received a copy of a Ph.D. thesis by M. Dahlem entitled "Disk-Halo Interactions in the Spiral Galaxies NGC 1808 and NGC 891" (Dahlem 1990). Figure 3.19 in that this is a map of the 20 cm polarization of NGC 891 made with the VLA in combined C and D configuration which shows an asymmetric distribution in the sense predicted by our model. A detailed comparison of that data with the results presented here will be of considerable interest.

Our results show that the magnetic fields in NGC 891 and NGC 4565 become progressively more ordered with increasing height above the plane. The direction of the magnetic field is predominantly parallel to the galactic plane in the central regions of the disks. In NGC 891 the field lines tilt away from the plane of the galaxy at large distances from the galaxy center. These conclusions are not sensitive to the amount of Faraday rotation or depolarization present in these galaxies.

We thank the staff of the VLA for their help and advice with the observations, and R. Sault and the staff of NCSA for their help with the data processing. We are grateful to A. Sandage for the optical images of the two galaxies, and to J. Bedke at ST ScI for carrying out the superposition of the radio contour maps on these images. S. S. was supported by the College of Liberal Arts and Sciences of the University of Illinois. Research on the structure of galaxies at Illinois was partly supported by The National Science Foundation under grant AST 8715905. R. J. A. thanks the staff of ST ScI for their advice and assistance. ST ScI is operated by the Association of Universities for Research in Astronomy, Inc., under contract NAS5-26555 with the National Aeronautics and Space Administration.

REFERENCES

Allen, R. J., Baldwin, J. E., & Sancisi, R. 1978, A&A, 62, 397
Allen, R. J., & Hu, F. X. 1985, in New Aspects of Galaxy Photometry, ed. J.-L. Nieto (New York: Springer), 293
Allen, R. J., & Sukumar, S. 1990, in The Interstellar Medium in External Galaxies: Summaries of Contributed Papers, ed. D. J. Hollenbach & H. A. Thronson (NASA CP-3084), 263
Allen, R. J., Sukumar, S., Hu, F. X., & Van der Kruit, P. C. 1990, in Galactic and Intergalactic Magnetic Fields, ed. R. Beck, P. P. Kronberg, & R. Wielebinski (Dordrecht: Kluwer), 223
Beck, R. 1991, in The Interstellar Disk-Halo Connection in Galaxies, ed. H. Bloemen (Dordrecht: Kluwer), in press
Broeils, A. H., & Sancisi, R. 1985, A&A, 153, 281
Burn, B. J. 1966, MNRAS, 133, 67–83
Danlem, M. 1990, Ph.D. thesis, Bonn University
de Vaucouleurs, G., de Vaucouleurs, A., & Corwin, H. G., Jr. 1976, Second Reference Catalogue of Bright Galaxies (Austin: Univ. of Texas)
Fujimoto, M. 1987, in Interstellar Magnetic Fields, ed. R. Beck & R. Gräve (New York: Springer), 23
Horellou, C., Beck, R., & Klein, U. 1990, in Galactic and Intergalactic Magnetic Fields, ed. R. Beck, P. P. Kronberg, & R. Wielebiniski (Dordrecht: Kluwer), 211
Hu, F. X., Allen, R. J., Van der Kruit, P. C., & You, J. H. 1987, Ap. Space Science, 135, 389
Hummel, E., Lesch, H., Wielebinski, R., & Schlickeiser, R. 1988, A&A, 197, L29
Krause, M., Beck, R., & Hummel, E. 1989, A&A, 217, 17
Lasker, B. M., Sturch, C. R., McLean, B. J., Russel, J. L., Jenkner, H., & Shara, M. M. 1990, AJ, 99, 2019
Rand, R. J., Kulkarni, S. R., & Hester, J. J. 1990, ApJ, 352, L1
Ruzmaikin, A. A., Dhukurov, A. M., & Sikoloff, D. D. 1988, Magnetic Fields of Galaxies (Dordrecht: Kluwer)
Sandage, A. 1961, The Hubble Atlas of Galaxies (Washington DC: Carnegie Institution)
Sofue, Y. 1987, in Interstellar Magnetic Fields, ed. R. Beck & R. Gräve (New York: Springer), 30
Sofue, Y., Fujimoto, M., & Wielebinski, R. 1986, ARAA, 24, 459
Sukumar, S., & Allen, R. J. 1989a, Nature, 340, 537
———. 1989b, ApJ, 341, 883
———. 1990, in Galactic and Intergalactic Magnetic Fields, ed. R. Beck, P. P. Kronberg, & R. Wielebinski (Dordrecht: Kluwer), 215
Sukumar, S., Klein, U., & Gräve, R. 1987, A&A, 184, 71
Wielebinski, R. 1990, in The Interstellar Medium in Galaxies, ed. H. A. Thronson & J. M. Shull (Dordrecht: Kluwer), 249